Potential collapse of the upper slope and tsunami generation on the Great Barrier Reef margin, north-eastern Australia

Ángel Puga-Bernabéu, Jody M. Webster & Robin J. Beaman

Natural Hazards
Journal of the International Society for the Prevention and Mitigation of Natural Hazards

ISSN 0921-030X

Nat Hazards
DOI 10.1007/s11069-012-0502-0

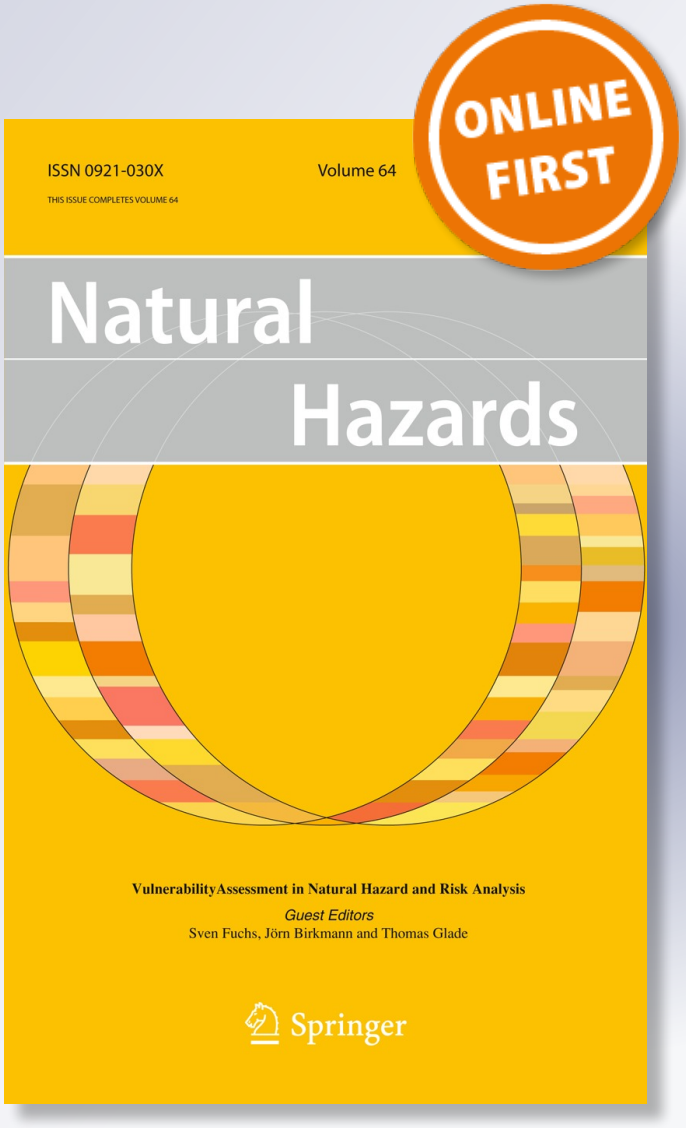

Springer

Nat Hazards
DOI 10.1007/s11069-012-0502-0

ORIGINAL PAPER

Potential collapse of the upper slope and tsunami generation on the Great Barrier Reef margin, north-eastern Australia

Ángel Puga-Bernabéu · Jody M. Webster · Robin J. Beaman

Received: 24 March 2012 / Accepted: 16 November 2012

Abstract Analysis of high-resolution multibeam bathymetry and seismic profiles in the Noggin Passage region, north-eastern Australia, has identified a small area (Noggin block) in the upper-slope offshore Cairns that may potentially collapse and generate a tsunami wave. The Noggin block extends from 340 to 470 m depth covering a roughly circular (2.4 km long and 3.7 km wide) area of about 5.3 km^2. The well-defined margins of the block correspond to different bounding seabed features. These features include steep headscarps, small landslides and a group of aligned circular pockforms up to 500 m wide and 20 m deep. Slope stability simulations indicate that the Noggin block is stable under normal present-day gravitational conditions on the upper slope. However, block failure may result under external loads, such as those produced by earthquakes. Failure modelling shows that critical peak horizontal accelerations of 0.2–0.4 g could lead to the collapse of the Noggin block. In north-eastern Australia, these acceleration values would involve earthquakes generated at short hypocentral distances and short periods. The collapse of the potential sediment slide mass of about 0.86 km^3 (162 m average thickness) may lead to the formation of a landslide-generated tsunami wave. Semi-empirical equations indicate the collapse of this mass would yield a 7–11-m high three-dimensional tsunami wave. These waves could reach an estimated run-up height at the coast of 5–7 m. Our first-order approach highlights the potential consequences for nearby coastal communities, the need for better sediment characterisation in the study area, and the systematic identification of other areas prone to slope failures along the Great Barrier Reef margin.

Á. Puga-Bernabéu (✉)
Departamento de Estratigrafía y Paleontología, Facultad de Ciencias, Universidad de Granada, Campus de Fuentenueva s.n., 18002 Granada, Spain
e-mail: angelpb@ugr.es

Á. Puga-Bernabéu · J. M. Webster
Geocoastal Research Group, School of Geosciences, University of Sydney, Sydney, NSW 2006, Australia

R. J. Beaman
School of Earth and Environmental Sciences, James Cook University, PO Box 6811, Cairns, QLD 4870, Australia

Published online: 25 November 2012

Keywords Slope failure · Tsunami run-up · Slope stability simulations · Coastal hazard · Landslide · Submarine canyons

1 Introduction

Submarine slope failure is a common process acting in different oceanographic settings (Hampton et al. 1996), and it plays an important role in shaping seafloor environments and the exchange of sediment between the shelf and the deep-sea basin (Canals et al. 2004). Triggered by diverse mechanisms (Sultan et al. 2004), submarine landslides have captured the attention of many researchers due to their potential to generate large and catastrophic tsunamis (Driscoll et al. 2000; Tappin et al. 2001; Fryer et al. 2004), and therefore, their study has important implications for assessing the potential tsunami hazard facing populated coastal areas.

The Australian coast has experienced modern tsunamis (Rynn and Davidson 1999; Dominey-Howes 2007), although the overall risk along this coast is lower than in many other parts of the world (Middelmann 2007). However, the Indian Ocean tsunami on 26 December 2004 highlighted the fact that large catastrophic tsunamis could potentially strike the Australia coastline. Since then, there has been an ongoing effort to understand the level of onshore hazard caused by tsunamis to the Australian coast (Sexton et al. 2009). Additional information is provided by the tsunami geological record (Bryant and Nott 2001) and probabilistic studies (Burbidge et al. 2008). Modelling studies have also provided a general context for the offshore (at the 100-m depth contour) tsunami hazard for Australia (Geoscience Australia 2008).

Most of the known Australian tsunamis have an earthquake-induced origin far from the Australian coast (Dominey-Howes 2007). For example, in 2007, the earthquake-generated (M_w 8.1) Solomon tsunami reached the north-eastern coast of Australia, but just as a small wave of less than 1 m in height (Queensland Government, Environment and Resource Management 2007). Numerical modelling suggests that the effects of the Solomon tsunami waves produced were diminished due to the refraction and reflection caused by the presence of the reef matrix of the Great Barrier Reef (Baba et al. 2008). However, landslide-induced tsunamis can be triggered much closer to the shore than co-seismic tsunamis generated far from the coast. So, despite their lower energy release (Ruff 2003), their high run-up and flooding may result in significant localised destruction along nearby coastlines (e.g. Sissano Lagoon, Papua New Guinea; Kawata et al. 1999; Synolakis et al. 2002).

Therefore, another step in the development of any tsunami hazard assessment on the Australian coastline is to develop a model describing other sources of tsunamis (e.g. submarine landslides), and the probability of that source in generating a tsunami of a given size at a given location. In this study, we have identified an area in the upper-slope offshore Cairns in north-eastern Australia that may potentially collapse and generate a tsunami wave. Here, we provide data about the location and morphology of this study block (herein called the Noggin block), basic slope stability simulations, an estimation of the maximum tsunami wave and run-up height, and discuss the triggering factors and the future investigations needed to test the reliability of any eventual slope failure.

2 Geological setting and sedimentology

The north-eastern Australia margin is a passive continental margin that constitutes a large depositional area of carbonate and terrigenous sediments, from shallow-water shelf

environments to deeper slope and basin settings. The study area is located in the central part of this margin, in the Noggin Passage region, about 100 km south-east offshore Cairns (Fig. 1). The shelf here is a gently dipping surface, about 65 km wide, with the shelf break located at about 102–109 m depth (Abbey et al. 2011). The outer shelf includes a series of submerged features such as barrier reefs, lagoons, pinnacles and terraces (Abbey et al. 2011; Webster et al. 2011). The shelf is connected to a moderately steep (4–7°) continental slope. Regionally, the slope is excavated by a submarine canyon system perpendicular to the shelf margin that extends to the base of the slope at about 1,400 m. The area studied in detail is located <5 km to the north of the Gloria Knolls landslide scarp (Beaman and Webster 2008; Webster et al. 2008a) and includes the slope areas surrounding Noggin Canyon 17 (Fig. 1).

Modern surface sediments on the slope and basin comprise terrigenous siliciclastic and bioclastic carbonates with a variable proportion and spatial distribution along the margin (Dunbar and Dickens 2003; Francis et al. 2007). Subsurface sediments comprise different sedimentary units that extend from the Pleistocene to the Middle Miocene (Davies et al. 1991). Slope sediments collected during the ODP Leg 133 (Sites 819, 820 and 821; Fig. 1) at similar depths to the study area (250–600 m) comprise Pleistocene units consisting of

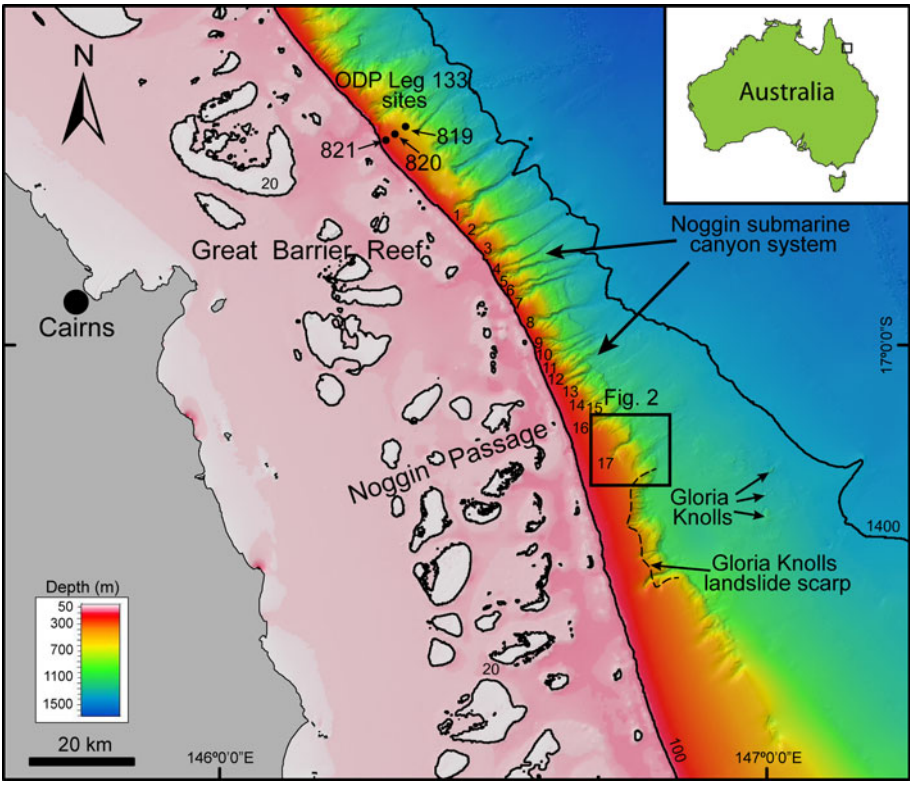

Fig. 1 Hillshade map of the study area in the Noggin Passage region, north-eastern Australia margin, from high-resolution multibeam data (RV *Southern Surveyor voyage* SS07/2007) and other data sources (see Beaman 2010). The continental margin offshore Cairns is shaped by a submarine canyon system and large-scale landslides. Canyons are *labelled* with *numbers*. *Inset* shows the location of the study area in detail. Location of ODP Leg 133, sites 819–821 is also *marked*

variable proportions of pelagic oozes, mixed carbonate-siliciclastic hemipelagic/pelagic sediments, and skeletal packstones, grainstones and floatstones (Davies et al. 1991). These units are organised in several fining- and coarsening-up sequences with increasing- and decreasing-up carbonate content. Although these ODP sites are located about 70 km to the north of the study area, it is reasonable to assume that this general subsurface stratigraphy extends to the study area.

3 Data and methods

Multibeam bathymetry and seismic reflection data were collected by the research vessel RV *Southern Surveyor* during September–October 2007 (SS007/2007; Webster et al. 2008a, b). The high-resolution bathymetry map was obtained using a Simrad EM300 multibeam echosounder (30 kHz), later processed using Caris HIPS and SIPS software and gridded to 30-m pixel resolution. Regional bathymetry data come from different sources and used to generate a 100-m resolution grid for the Great Barrier Reef and Coral Sea (Beaman 2010). Bathymetry grids were imported into ESRI ArcMAP 9.3 to create slope maps and bathymetric profiles. Digital elevation models (DEMs) were generated using Fledermaus V7.2.1 software. All these datasets were used to study the detailed surface morphology and 3D structure of the Noggin block. Seismic reflection data were acquired from the continental slope using Topas PS18. The SEG file profiles were imported to Kingdom V8.6 software for visualisation and interpretation. Submarine canyons identified within the Noggin Passage region have been numbered from north to south (Fig. 1).

Geomechanical models for the potential failure of the study block were run with Slope/W software, by means of the generalized limit equilibrium (GLE) method (Fredlund and Krahn 1977; Fredlund et al. 1981). Several depth profiles were produced in order to simulate possible scenarios of instability development and to determine the initial slide plane. The position of the most critical initial failure surface was constrained using a wide range of entry and exit points at the slope. Static simulations were firstly simulated, followed by simulations under seismic loadings using the pseudo-static method, which considers the seismic accelerations in terms of equivalent static forces (Terzaghi 1950). In both cases, a factor of safety (FoS), defined as the ratio of the resisting forces to the disturbing forces, was determined. The effect of other destabilising processes, such as fluid or gas seepage on slope stability, has not been included in these simulations; however, they are considered within the discussion.

4 Results

4.1 Slope and block morphology

4.1.1 Slope

The study area covers the slope around Noggin Canyon 17 (Fig. 1) between 150 and 1,250 m depth (Fig. 2). The head of this canyon is excavated into a gently inclined (<2.5°) upper-slope shoulder to seawards from the modern shelf break at between 102 and 109 m depth. This uppermost slope area extends down to about 250–300 m where the gradient then becomes steeper. Depth profiles show a gaussian (sigmoidal) slope, with the steepest

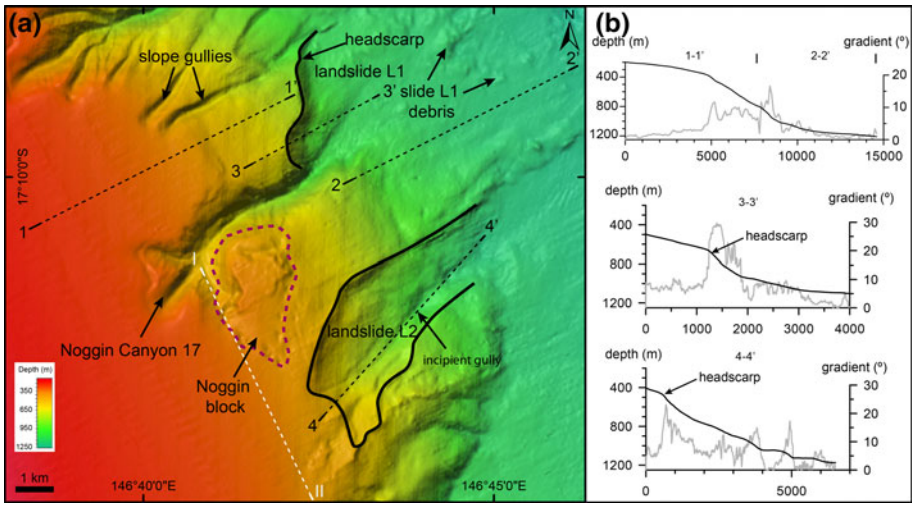

Fig. 2 **a** Hillshade map of the study area in detail, from high-resolution multibeam data (SS07/2007) and gridded at 30 m. This study focused on the area close to the Noggin Canyon 17 (Noggin block; *dotted line*). This block covers an area of about 5.3 km^2 in the upper slope. Adjacent landslides and debris indicate that slope failure is a common process in this region. *Black dashed lines* indicate the position of depth profiles shown on the *right*. *White dashed line* marks the location of the seismic line shown in Fig. 4. **b** Depth (*black*) and gradient (*dashed grey*) profiles along selected locations. Composed profile 1–2 shows the sigmoidal shape of the original slope. Profiles 3 and 4 illustrate the morphology of the slope shaped by landslides L1 and L2, respectively

gradients (8°–16°) between 300 and 1,100 m, and then decreasing at deeper waters with gradients less than 4° (Fig. 2b).

In the study area, downslope from the canyon area, several slope failures have modified the seafloor morphology. Two main submarine landslides (L1 and L2) are observed in the middle and lower slope nearby the canyon valley. The northern slope failure (L1) comprises a 3-km wide headscarp between 650 and 900 m depth (Fig. 2 profile 3–3′). This steep (24°–26°) headscarp has a surficial height of 150–250 m and is partly connected with the lower canyon. Downslope from the headscarp, the seafloor is covered with collapsed debris of various sizes, several 100 s of m long and a few m high. The southern landslide (L2) consists of a 2-km wide spoon-shaped feature starting at 400 m and extending to the base of the slope with an average gradient of 10° (Fig. 2 profile 4–4′). This feature also shows a narrow gully located through its axis, and small debris found at the base of the slope. Narrow slope gullies are also observed to the north of Noggin Canyon 17.

In addition, a much larger slope failure, known as the Gloria Knolls landslide scarp, is located south of the study area (Fig. 1). This landslide significantly modified the shelf and slope areas by removing about 32.6 km^3 of material (Beaman and Webster 2008).

4.1.2 Noggin block

Starting at a depth of 340 m and extending down to 470 m, a 2.4-km long and 3.7-km wide sediment block has been identified at southern part of the head of Noggin Canyon 17. The centre of the block is located at 17°11.44′S, 146°41.62′E (Figs. 2, 3a). This block has a roughly circular shape, covering an approximate area of 5.3 km^2 in the upper slope, and is easily distinguished from the surrounding slope area. The margins of the block are clearly

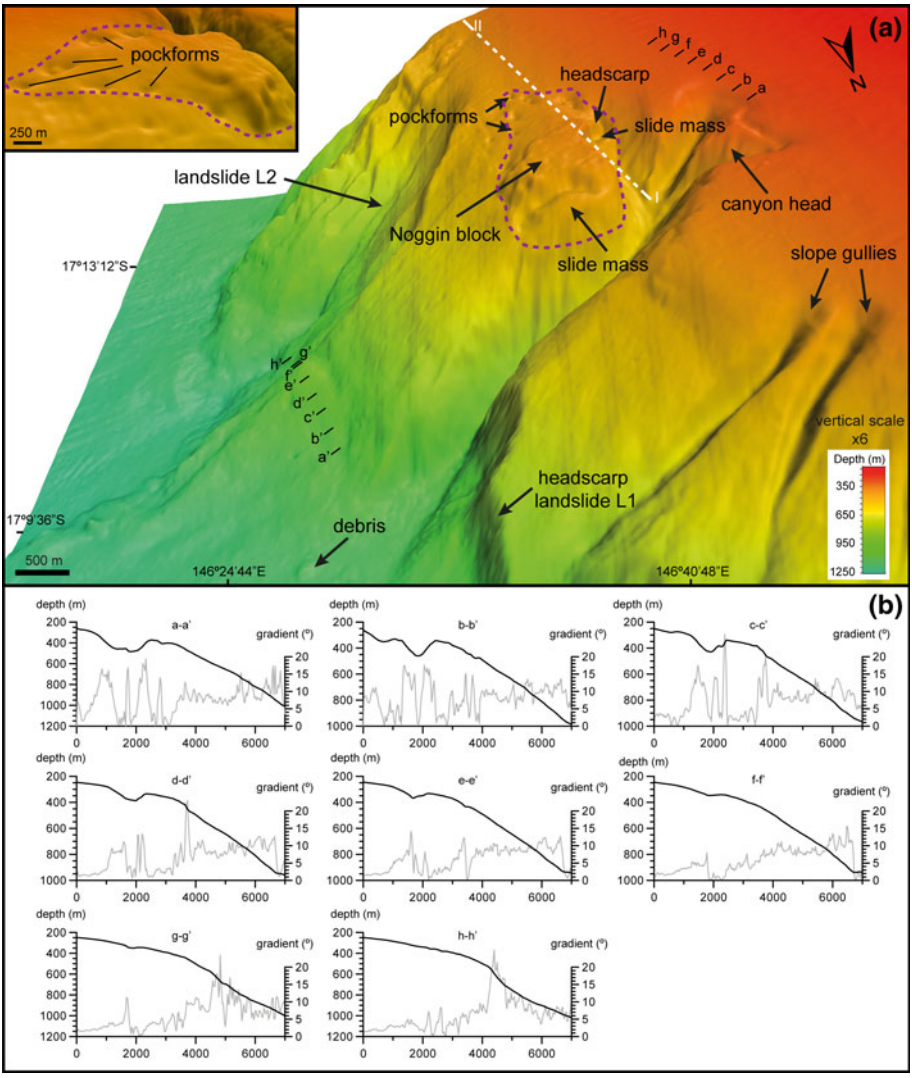

Fig. 3 **a** Southerly looking 3D view of the Noggin block site and location of depth profiles across this block. Seismic profile shown in Fig. 4 is marked as a *white line* (I–II). The block is limited by a series of pockforms (see *upper left inset*), headscarps and a canyon branch that suggests sediment disruption and destabilisation processes. These processes are also revealed by the presence of adjacent slope failures. **b** Depth (*black*) and gradient (*grey*) profiles across the study block used in slope stability simulations

defined in the bathymetry data by different bounding features (Fig. 3a). The northern flank of the block corresponds to a headscarp 20 m in height, with a gradient of 9°, and partly forms the southern wall of Noggin Canyon 17. To the east, the block has a steep flank of about 15° that passes downward to an 8° slope. The southern boundary is defined by several aligned circular depressions (pockforms) <500 m apart. These depressions are 100–500 m long and 5–20 m deep, increasing in size from east to west. The western flank of the block is connected to one of the canyon branches. On part of this northern side

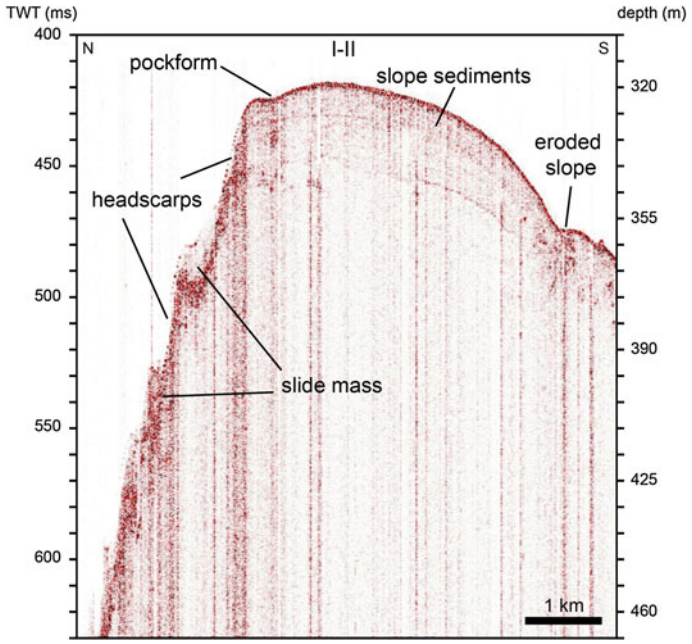

Fig. 4 Seismic line (SS072007_012_003) along the slope showing part of the western boundary of the Noggin block. This profile shows small slide masses with steep headscarps close to Noggin Canyon 17 and a pockform

boundary, there appears to be a small slide (Fig. 4), leaving a headscarp surface up to 40 m in height and gradients of 15°–18°.

4.2 Slope stability and failure simulations

High-resolution bathymetry has allowed us to define the surface boundaries of the Noggin block on the seafloor. Slope stability and failure modelling were simulated in several depth profiles across the block and slope (Fig. 3b) in order to delimit the lower surface or the most critical slide plane in the case of block collapse. In the absence of direct measurements of sediment strength parameters (cohesion and friction angle), modelling scenarios were carried out using a range of strength values for the sediments in the study area. In each case, effective friction angles of 30°, 25°, 15°, 7.5° and 3.75° were used in a Mohr–Coulomb strength model (Table 1). A cohesion value of 0 kPa was initially used for all simulations with these friction angles. Additional scenarios with increasing sediment cohesion and peak friction angles were also simulated. Although sediment cores from the study area are not available, the unit weight of slope sediments can be considered similar to that of sediments drilled in comparable slope settings from ODP Leg 133 Site 820 (Davies et al. 1991). In this site, the first 150 m below the seafloor corresponds to a bioclastic unit that comprises unlithified, very fine, sand-sized wackestones and mudstones, interbedded with bioclastic packstones. Average grain density in this interval is 2.75 g/cm^3, with porosity values ranging from 40 to 68 % (average 51.75 %), and void ratios from 0.66 to 2.11 (average 1.10). These parameters provide an estimated average unit weight (γ) of 18 kN/m^3 (15–21 kN/m^3).

Table 1 Strength parameters and resulting factor of safety (FoS) obtained in slope stability simulations for different profiles across the study block (Fig. 3)

Cohesion (kPa)	Friction angle (°)	FoS							
		Profile a–a′	Profile b–b′	Profile c–c′	Profile d–d′	Profile e–e′	Profile f–f′	Profile g–g′	Profile h–h′
0	30	5.024	5.03	4.666	4.496	4.775	4.501	4.227	3.617
	25	4.058	4.062	3.769	3.631	3.857	3.635	3.414	2.921
	15	2.332	2.334	2.166	2.086	2.216	2.089	1.962	1.679
	7.5	1.146	1.147	1.064	1.025	1.089	1.026	*0.964*	*0.825*
	3.75	*0.57*	*0.571*	*0.53*	*0.476*	*0.542*	*0.511*	*0.48*	*0.411*
1.25	30	5.883	5.864	5.595	5.403	5.743	5.565	5.65	4.584
2		6.399	6.365	6.152	5.936	6.324	6.084	6.096	4.988
5		8.3	8.107	7.463	7.176	7.89	7.432	7.861	6.604
10		10.629	10.327	9.55	9.223	10.132	9.679	10.803	9.297
22	30	16.219	15.578	14.56	14.105	15.514	15.01	17.865	15.76
	25	15.07	14.433	13.527	13.113	14.428	14.002	16.919	15.008
	15	12.989	12.389	11.68	11.342	12.459	12.203	15.23	13.665
	7.5	11.546	10.978	10.412	10.119	11.105	10.967	14.069	12.745
	3.75	10.845	10.283	9.797	9.519	10.449	10.366	13.506	12.295
	0	10.151	9.594	9.187	8.924	9.798	9.762	12.949	11.851

Italicized values correspond to unstable conditions

Slope stability results (Table 1) indicate that the Noggin block is stable under the general static conditions simulated. Only simulations with no sediment cohesion (c) and low-friction angles ($\varphi = 3.75°$–$7.5°$, Table 1) produce unstable conditions with a FoS < 1. Therefore, some other destabilizing processes are necessary in order to trigger the collapse of the Noggin block.

The effect of seismic loading on the sediment slope stability was also simulated. Seismic shaking simulations were run using undrained conditions ($\varphi = 0$) in order to simulate short-term, rapid dynamic loading, and considering sediment cohesion of 1, 10 and 22 kPa. Increasing horizontal accelerations (K_h, expressed as a portion of the gravity acceleration) were applied to the sediment until achieving a FoS < 1 (Table 2). The slope stability under the action of an external load, such as an earthquake, is conditioned by the sediment cohesion (Fig. 5). Simulations show that the Noggin block would collapse under horizontal accelerations between 0 and 0.5 g depending of the sediment cohesion (Fig. 5).

The geometry of the modelled slide under different seismic loading conditions is shown in Fig. 6a. Profile d–d′ was selected to show the morphology of the slide plane as it crosses the middle of the Noggin block (Fig. 3). The most critical scenario under seismic shaking ($c = 10$ kPa, undrained conditions and $K_h = 0.2$ g) leads to the formation of a very deep slide surface, involving a slide mass of up to 600 m thick (top slide in Fig. 6a). This geometry does not match the geometry of adjacent landslides (L1 and L2) found in the study area (Fig. 6b). However, simulations with a $K_h = 0.4$ g with FoS between 0.879 and 0.986 (unstable conditions) generate slide geometries more similar to those in adjacent landslides (middle slide in Fig. 6a). Similar surfaces are also found in simulations under drained conditions ($\varphi = 30$, $c = 0$) and moderate seismic horizontal accelerations ($K_h = 0.2$ g) (bottom slide in Fig. 6a).

Table 2 Factor of safety (FoS) obtained in slope stability simulations in different depth profiles under various horizontal accelerations produced by seismic events

k_h	Cohesion (kPa)											
	Profile a–a'			Profile b–b'			Profile c–c'			Profile d–d'		
	1	10	22	1	10	22	1	10	22	1	10	22
0	*0.461*	4.614	10.151	*0.436*	4.631	9.594	*0.418*	4.176	9.187	*0.406*	4.056	8.924
0.1	*0.144*	1.443	3.174	*0.138*	1.383	3.042	*0.141*	1.413	3.108	*0.113*	1.424	3.133
0.2		*0.849*	1.868		*0.817*	1.798		*0.839*	1.847		*0.851*	1.872
0.3		*0.598*	1.315		*0.577*	1.270		*0.594*	1.307		*0.599*	1.317
0.4			1.014			*0.981*			1.005			1.015
0.5			*0.825*			*0.799*			*0.815*			*0.825*
0.6												
0.7												

k_h	Cohesion (kPa)											
	Profile e–e'			Profile f–f'			Profile g–g'			Profile h–h'		
	1	10	22	1	10	22	1	10	22	1	10	22
0	*0.445*	4.454	9.798	*0.444*	4.437	9.762	*0.589*	5.886	12.949	*0.539*	5.387	11.851
0.1	*0.146*	1.458	3.207	*0.151*	1.507	3.314	*0.211*	2.107	4.673	*0.211*	2.116	4.656
0.2		*0.863*	1.900		*0.886*	1.949		1.255	2.760		1.299	2.859
0.3		*0.608*	1.337		*0.626*	1.378		*0.892*	1.962		*0.936*	2.058
0.4			1.031			1.064			1.520			1.606
0.5			*0.838*			*0.867*			1.238			1.314
0.6									1.045			1.112
0.7									*0.903*			*0.963*

Simulations were run considering undrained conditions and different sediment cohesion values. Italicized values correspond to unstable conditions

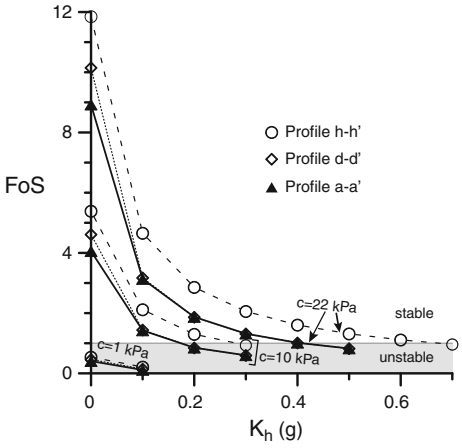

Fig. 5 Factor of safety (*FoS*) for simulated slope failures across selected depth profiles (Fig. 3) under seismic loading (horizontal acceleration K_h) expressed as a portion of gravity acceleration. Slope is more stable with increasing sediment cohesion. Note that the most probable sediment cohesion values (10 kPa) suggest slope instability under horizontal accelerations higher than 0.2 g

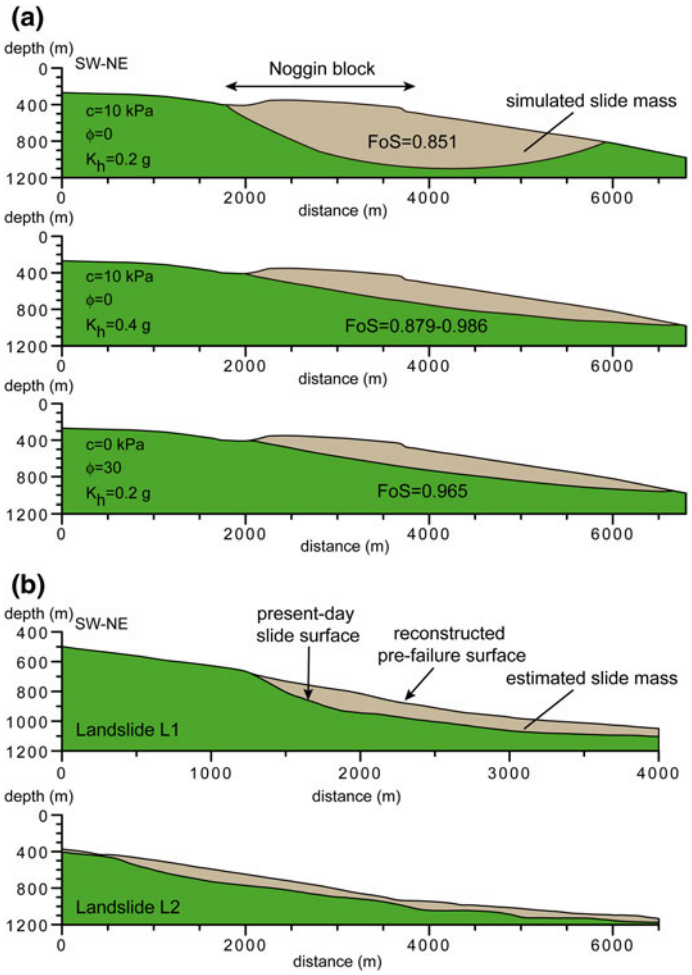

Fig. 6 **a** Depth profiles (d–d′) showing the geometry of the modelled slide mass and location of the study block. Simulated slide surfaces correspond to undrained ($\varphi = 0$) and drained ($\varphi = 30$) conditions, different horizontal accelerations and cohesion values. **b** Reconstructed depth profiles across landslides L1 and L2 showing the geometry of the slide mass. Note that some instable simulated geometries in **a** are comparable in size and shape to the geometries of previously failed slopes

4.3 Tsunamigenic potential

Modelled surfaces with similar geometries to the adjacent landslides indicate a significant volume of sediment up to 250 m thick (162 m average; Fig. 6) could slide under adequate conditions. Considering the average thickness, the slope stability simulations involve a potential sediment slide mass of about 0.86 km^3. The collapse of such a sediment mass may lead to the formation of a landslide-generated tsunami wave.

Many tsunami generation and run-up models have been developed, including some specifically applied to submarine mass failures. In this study, in order to estimate the tsunami wave amplitude that could be generated over the top of the eventual slide of the Noggin block, semi-empirical equations based on two- and three-dimensional numerical

simulations have been used (Grilli et al. 2002; Grilli and Watts 2005; Watts et al. 2005). We have assumed the simplest case, a translational slide. For translational slides with no basal friction, and strong fluid dynamic drag, the maximum three-dimensional tsunami amplitude (η_o) is given by Grilli et al. (2002), Grilli and Watts (2005), Watts et al. (2005):

$$\eta_o = S_o(0.0574 - 0.0431\sin\theta)\left(\frac{T}{b}\right)\left(\frac{b\sin\theta}{d}\right)^{1.25}\left(1 - e^{-2.2(s-1)}\right)\left(\frac{w}{w+\lambda_o}\right) \quad (1)$$

where S_o is the distance of motion for translational failures,

$$S_o = \frac{\pi}{2}b(s+1) \quad (2)$$

θ is the angle of the slope, T is the maximum thickness of the failed mass, b is the length of the slide mass, d the average depth above the centre of the slide mass, s is the sediment-specific gravity, w the slide mass width and λ the tsunami wavelength,

$$\lambda_o = \sqrt{\frac{\pi b d(s+1)^2}{2\sin\theta(s-1)}} \quad (3)$$

Table 3 provides the selected parameters for the study case and calculated tsunami amplitude, distance of motion and tsunami wavelength following Eqs. (1)–(3). These numerical equations are valid within a range of $\theta \in [5,30°]$, $d/b \in [0.06,1.5]$, $T/b \in [0.008,0.2]$ and $s \in [1.46,2.93]$ which are satisfied by values expressed in Table 3. Two different scenarios were considered: Case 1, a slide thickness equal to a simulated thickness ($T = 250$ m), which is similar to the material failed in adjacent landslide L1; and Case 2, a slide thickness of 150 m, which is about the value of the estimated failed mass in adjacent landslide L2 (Fig. 5b). According to the predictive equations above, the mass failure of the Noggin block would yield at the generation point a characteristic three-dimensional tsunami wave elevation of about 11.2 m for the first case and a 6.7-m elevation for the second case. Therefore, we can expect tsunami amplitudes at the origin of between about 7–11 m.

The estimated maximum tsunami amplitude is considered to be similar to the maximum tsunami run-up ($R \approx \eta_o \approx$ 7–11 m) according to the correspondence principle (Watts et al. 2003, 2005). However, due to shoaling and amplification effects, run-up height is usually higher than the tsunami wave height at the origin. For long waves and following the Green's Law, Ward (2011) proposes that the run-up height (R) can be broadly estimated by:

$$R = \eta_o(d)^{4/5}d^{1/5} \quad (4)$$

with $\eta_o(d)$ the wave amplitude at depth d. This approach yields a run-up height of 16.5–24.5 m at the coast for initial waves of 7 and 11 m, respectively (Table 3).

Table 3 Input parameters for simulated study block landslide and estimated output tsunami characteristics for two study cases

Parameter	s	T (m)	b (m)	w (m)	d (m)	θ (°)	S_o (m)	λ_o (m)	η_o (m)	R (m)
Case 1	1.85	250	4,900	3,500	600	9	21,936	16,796	11.2	24.5
Case 2	1.85	150	4,900	3,500	600	9	21,936	16,796	6.7	16.5

s sediment-specific gravity, T maximum thickness of the failed mass, b length of the slide mass, w width of the slide mass, d average depth above the centre of the slide mass, θ angle of the slope, S_o distance of motion, λ_o tsunami wavelength, η_o, three-dimensional tsunami amplitude, R tsunami run-up

The site-specific effects on tsunami wave propagation along the adjacent coast are here complicated by the presence of coral reefs. Baba et al. (2008) simulated the propagation of the 2007 Solomon Island tsunami into the GBR and found that the coral reefs decreased the amplitude of the first incoming wave by half or less. If we apply such a decrease to the Noggin block case, a tsunami wave 3.5–5.5 m high would still generate a significant run-up at the adjacent coast (about 5–7 m for an average water depth of 20 m). More accurate run-up estimations would need precise data including period, size and direction of the incoming waves, number of waves, beach and coastal morphology and bottom friction, which are beyond the scope of this study.

5 Discussion

5.1 Block collapse

Our morphological analysis of the high-resolution bathymetry data offshore Cairns, north-eastern Australia, has identified a well-defined area in the upper slope that could collapse under certain conditions. This area is characterized by a group of small, aligned, circular seabed features (pockforms) and by headscarps with slide masses clearly observed at their base (Fig. 3a). These seafloor features are indicative of sediment disruption, probably suggesting initial destabilisation processes, and can be considered as a precursor to a larger sediment failure.

Within the previously stated data uncertainties, the slope stability simulations show that the Noggin block is apparently stable under normal present-day gravitational conditions on the upper slope. However, instability conditions were found when seismic loading was considered. Calculated critical earthquake accelerations that may trigger the Noggin block failure range from 0 to 0.5 g, depending on the assumed sediment cohesion. The most realistic scenario considers a maximum cohesion value of 10 kPa for the slope sediments, as the slide plane geometries observed in adjacent landslide scarps are similar to those simulated in failure analyses. This maximum value is also in agreement with values of 0–9.57 kPa for marine, low-energy, fine-grained sediments (Koloski et al. 1989), and with values used in some slope stability models dealing with hemipelagic slope sediments (7 kPa, Urgeles et al. 2007). Peak horizontal accelerations (PHA) of 0.2–0.4 g are necessary to trigger the failure of the Noggin block considering a sediment cohesion of 10 kPa.

In Australia, as in other tectonically stable margins, the estimation of earthquake ground shaking effects is limited due to the paucity of data, especially for large earthquakes. Recently, Australian-specific ground-motion prediction equations (GMPE; McPherson and Allen 2006; Somerville et al. 2009) show that these equations are consistent with the western North American GMPE of Chiou and Youngs (2008). Using these equations, and considering that the maximum earthquake magnitude elsewhere in Australia is estimated to be M_W 7.0–7.5 $\pm$ 0.2 (Allen et al. 2011), earthquakes that may produce peak ground accelerations (maximum horizontal acceleration at ground surface induced by an earthquake) of 0.2–0.4 g should generate at short hypocentral distances and short periods (Table 4). Figure 7 shows the occurrence of earthquakes in the Cairns region in recent times (1866–2011; Earth Systems Science Computational Centre (2011); Geoscience Australia 2012). Many of these earthquakes have occurred in offshore areas underneath the shelf and upper slope at relatively short distances from the study area (<50 km). Overall, these earthquakes are of too low magnitude to generate the critical peak horizontal acceleration. However, the occurrence of unexpected larger seismic events able to trigger

Table 4 Estimated peak horizontal accelerations produced by earthquakes of different magnitude, period and hypocentral distance using ground-motion prediction equations of Chiou and Youngs (2008)

	$M_w = 5$			$M_w = 5.4$			$M_w = 6.0$						$M_w = 7.0$					
PHA (g)	0.2	0.2	0.4	0.2	0.2	0.4	0.2	0.2	0.2	0.4	0.4	0.4	0.2	0.2	0.2	0.4	0.4	0.4
Rx (km)	<5	6–13	<6	10	10	10	8–15	16–28	6–16	<8	<16	<6	18–28	30–50	15–35	<18	<30	<15
P (s)	0.01	0.2	0.2	0.02	0.2	0.1	0.01	0.2	1.0	0.01	0.2	1.0	0.01	0.2	1.0	0.01	0.2	1.0

Mw moment magnitude, *PHA* peak horizontal acceleration, *Rx* hypocentral distance, *P* period

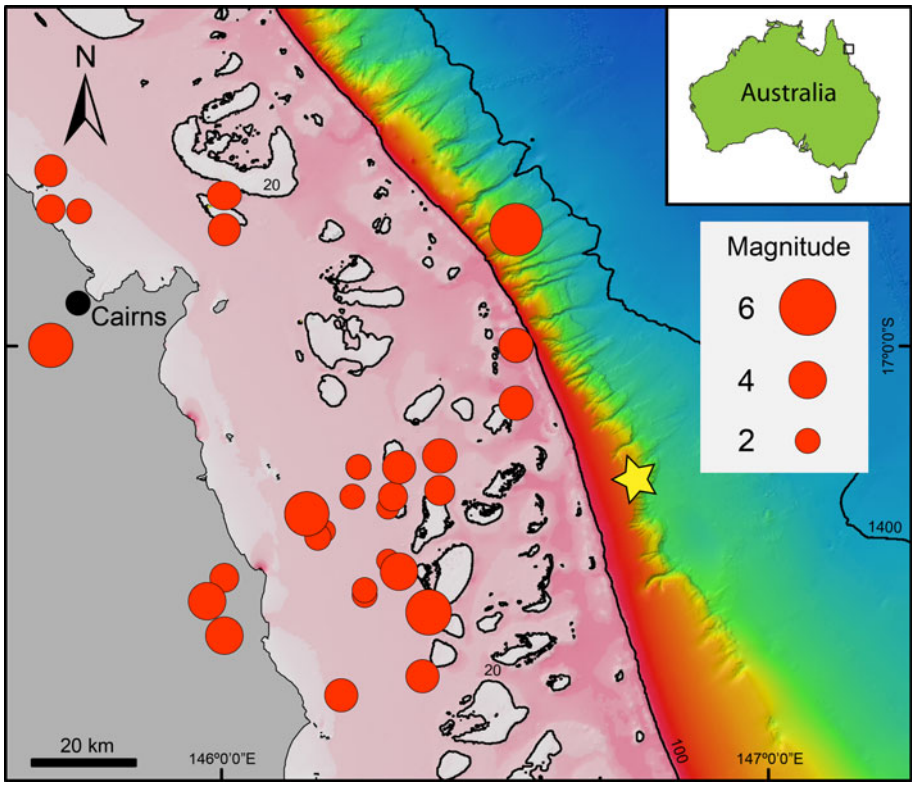

Fig. 7 Hillshade map of the study area offshore Cairns showing the distribution and magnitude of earthquakes events from 1866 to 2011 (Earth Systems Science Computational Centre; Geoscience Australia). *Yellow star* marks the location of the Noggin block. Observe that some of these recent earthquakes have occurred relatively close to the Noggin block at <50 km

the study block collapse cannot be discarded based only on the available recent earthquake record. Furthermore, amplification effects due to local site conditions could increase the local peak horizontal acceleration value (Venkatesan et al. 2003).

5.2 Tsunami generation and run-up heights

Based on slope stability simulations and equations derived from numerical models, a tsunami wave about 7–11 m high could be generated in case of the catastrophic collapse of the Noggin block. Although the area and sediment volume that could potentially be mobilised during the landslide is small compared to other well-known large tsunamigenic landslides (Moore et al. 1989; Fryer et al. 2004; Haflidason et al. 2004), similar tsunami amplitudes corresponding to comparable or even smaller slide mass volume have been estimated or modelled in other continental margins around the world (Rabinovich et al. 2003; McAdoo and Watts 2004; Tinti et al. 2007).

Although the site-specific effects on potential tsunami wave propagation controlled by the local bathymetry and topography (here complicated by the presence of coral reefs) are not included our simulations, the predicted coastal run-up heights do provide a tool for the estimation of tsunami hazards in nearby coastal communities. Considering an approximate

and variable tsunami wave speed ($s = \sqrt{gd}$) of about 20–370 km/h depending on the range of shelf depths traversed, and that the nearest coastline is located at about 70 km from the point source, the modelled tsunami wave would reach the coast in about 1 h. Despite the sparse population along the coast here, more detailed tsunami modelling using a landslide source is recommended.

5.3 Triggering mechanisms

Slope stability simulations have shown that the Noggin block is stable under static gravitational loading and that the block failure needs an external load; for example, the seismic loading modelled here. Other factors, such as high sedimentation rates or gas hydrate dissociation, may influence the static conditions (Baraza et al. 1990; Kayen and Lee 1991; Nixon and Grozic 2006) by increasing the pore pressure in the sediment and thus reducing the sediment stability. The presence of high pore pressures generated by groundwater seepage may also trigger the Noggin block failure. Such a groundwater flow regime has not been found in the study area due to the lack of available seismic data. However, the presence of pockforms bounding the study block and adjacent slopes (Fig. 3a) suggests that this possibility cannot be dismissed as a trigger and needs further research.

5.4 Limitations, constraints and future work

This study represents a first step towards a more detailed investigation of slope failure dynamics and landslide-generated tsunami risk along the north-eastern Australia margin. Uncertainties in our models relate mainly to input parameters due to the lack of available data in the study area. Slope stability analyses assume a single layer of sediment with uniform characteristics (cohesion, friction angle, unit weight). This may seem a simplistic approach but even if short sediment cores were available, they would only provide information about the geotechnical properties in the uppermost few m of the sediment column, and therefore their variation with depth would still have to be estimated. Thus, a single layer method using common strength values for upper-slope sediments can be considered as a good starting point to recognise slope instabilities and thus represents the worst-case scenario for a mass failure.

Another uncertainty concerns the triggering mechanism. Considering localised earthquakes as the potential triggering factor, we have simulated the short-term, rapid dynamic loading by considering undrained conditions. However, the influence of this rapid dynamic loading could also be evaluated by performing analyses of cyclic loading conditions which can significantly increase the pore pressure and reduce sediment strength (Baraza et al. 1990; Leynaud et al. 2004). But, again, this requires in situ sediment property data to estimate the over-consolidation ratio. Uncertainties derived from the limited ground motion models in north-eastern Australia further influence the probability of occurrence of the triggering seismic event.

One important factor that conditions the characteristic of a landslide-generated tsunami wave is the initial acceleration of the failed mass, and the landslide kinematics depends on the stress state and the shear strength properties of the sediment (Harbitz et al. 2006; Bradshaw et al. 2007). Although such factors, as well as the influence of the local bathymetry and basal friction on the run-up height (Li and Raichlen 2003; Gedik et al. 2005; Hsiao et al. 2008), are necessary to conduct precise numerical modelling in local areas, these models can benefit from the initial approach presented in this study. The

propagation of the incoming tsunami wave will likely attenuate due the complex reef system in the GBR. However, our approach may represent the worst-case scenario, and therefore, this study area could be considered for further detailed tsunami risk assessment.

Evidence of other slope landslides on the GBR margin has been identified with failed areas up to 178 km^2 in area and about 32 km^3 in volume of collapsed material, such as the Gloria Knolls landslide scarp located about 5 km south of the Noggin block (Beaman and Webster 2008; Puga-Bernabéu et al. 2011). This large slope failure is similar in scale to submarine landslides identified along the New South Wales margin, south-eastern Australia, which are considered as tsunamigenic landslides (Glenn et al. 2008). The potential collapse of the smaller-scale Noggin block may represent a local, small point source for tsunami generation, but given the presence of much larger slope failures in adjacent areas, its importance at the regional scale cannot be dismissed.

In summary, while our modelling approach needs better characterisation of the in situ but currently unavailable sediment properties, we have identified an area of potential instability area on the upper slope of the GBR margin. Our first-order simulations of slope failure and the resulting tsunami wave highlight the potential consequences for nearby coastal communities, while underscoring the need for further study. Future effort should focus on obtaining detailed sediment core and subsurface geophysical information over the study area, along with obtaining more comprehensive high-resolution multibeam coverage of the entire GBR margin to identify other areas prone to slope failures.

6 Conclusions

Based on our detailed morphologic analysis of high-resolution bathymetric data, slope stability simulations and semi-empirical equations, we draw the following conclusions:

1. The Noggin block covers an area of 5.3 km^2 in the upper-slope offshore Cairns. This block is bounded by headscarps, slide sediment masses and a group of aligned circular depressions. These seabed features are indicative of sediment disruption and can be considered as the precursors of a larger sediment failure.
2. Slope stability simulations indicate that the Noggin block is stable under present-day normal gravitational conditions on the upper slope. However, destabilizing external forces such as earthquakes may lead to the collapse of the Noggin block.
3. Critical peak horizontal accelerations of 0.2–0.4 g would lead to the failure of the Noggin block. In north-eastern Australia, these values would correspond to earthquakes generated at short hypocentral distances and short periods, which have not been observed in instrumental records (i.e. the last 150 years).
4. The potential collapse of the Noggin block (about 0.86 km^3) could generate a three-dimensional tsunami wave height of about 7–11 m at the inception point. Such a wave would reach a maximum run-up height of 16.5–24.8 m at the nearby coast. However, the complex reef morphology of the GBR shelf would likely attenuate the incoming tsunami and reduce either the tsunami height or the run-up by half or less.

Acknowledgments This research was supported by a James Cook University Faculty Grant Scheme, University of Sydney Start-Up funding, the Australian Marine National Facility for RV *Southern Surveyor* shiptime, National Geographic Society and the Natural Environment Research Council. APB was additionally funded by a Research Contract of the Universidad de Granada (Spain). RJB acknowledges a Queensland Smart Futures Fellowship for salary support. Constructive reviews by two anonymous reviewers are greatly appreciated.

References

Abbey E, Webster JM, Beaman RJ (2011) Geomorphology of submerged reefs on the shelf edge of the Great Barrier Reef: the influence of oscillating Pleistocene sea-levels. Mar Geol 288:61–78. doi:10.1016/j.margeo.2011.08.006

Allen TI, Burdidge DR, Clark D, McPherson AA, Collins, CDN, Leonard M (2011) Development of the next generation Australian National Earthquake Hazard Map. In: Proceedings of the ninth pacific conference on earthquake engineering, building and earthquake-resilient society, Auckland, New Zealand, paper 207, p 8

Baba T, Mleczko R, Burbidge D, Cummins P, Thio HK (2008) The effect of the Great Barrier Reef on the propagation of the 2007 Solomon Islands tsunami recorded in north-eastern Australia. Pure Appl Geophys 165:2003–2018

Baraza J, Lee HJ, Kayen RE, Hampton MA (1990) Geotechnical characteristics and slope stability on the Ebro margin, western Mediterranean. Mar Geol 90:379–393

Beaman RJ (2010) 3DGBR. A high-resolution depth model for the Great Barrier Reef and Coral Sea. Marine and Tropical Sciences Research Facility (MTSRF) Project 2.5i.1a Final Report, Reef and Rainforest Research Centre, Cairns, Australia, p 13 plus Appendix 1. Data available from: http://www.deepreef.org/bathymetry/65-3dgbr-bathy.html

Beaman RJ, Webster JM (2008) Gloria Knolls: a new coldwater coral habitat on the Great Barrier Reef margin. 4th International symposium on deep-sea corals, National Institute of Water and Atmospheric Research, Wellington, New Zealand, p 248

Bradshaw AS, Baxter CDP, Taylor O-DS, Grilli S (2007) Role of soil behavior on the initial kinematics of tsunamigenic slides. In: Lykousis V, Sakellariou D, Locat J (eds) Submarine mass movements and their consequences. Springer, Berlin, pp 387–394

Bryant EA, Nott J (2001) Geological indicators of large tsunami in Australia. Nat Hazards 24:231–249

Burbidge D, Cummins PR, Mleczko R, Thio HK (2008) A probabilistic tsunami hazard assessment for western Australia. Pure Appl Geophys 165:2059–2088

Canals M, Lastras G, Urgeles R, Casamor JL, Mienert J, Cattaneo A, De Batist M, Haflidason H, Imbo Y, Laberg JS, Locat J, Long D, Longva O, Masson DG, Sultan N, Tricardi F, Bryn P (2004) Slope failure dynamics and impacts from seafloor and shallow sub-seafloor geophysical data: case studies from the COSTA project. Mar Geol 213:9–72

Chiou BS-J, Youngs RR (2008) An NGA model for the average horizontal component of peak ground motion and response spectra. Earthq Spectr 24:173–215

Davies PJ, McKenzie JA, Palmer-Julson A, ODP Leg 133 Scientific Party (1991) Proceedings of Ocean Drill Program Initial Rep 133. Ocean Drilling Program, College Station, TX (Ocean Drilling Program)

Dominey-Howes D (2007) Geological and historical records of tsunami in Australia. Mar Geol 239:99–123

Driscoll NW, Weissel JK, Goff JA (2000) Potential for large-scale submarine slope failure and tsunami generation along the U.S. mid-Atlantic coast. Geology 28:407–410

Dunbar GB, Dickens GR (2003) Late quaternary shedding of shallow-marine carbonate along a tropical mixed siliciclastic-carbonate shelf: Great Barrier Reef, Australia. Sedimentology 50:1061–1077

Earth Systems Science Computational Centre (2011) University of Queensland. Queensland earthquake map, Cairns region. http://www.quakes.uq.edu.au. Accessed 10 Nov 2011

Francis JM, Dunbar GB, Dickens GR, Sutherland IA, Droxler AW (2007) Siliciclastic sediment across the North Queensland Margin (Australia): a Holocene perspective on reciprocal versus coeval deposition in tropical mixed siliciclastic-carbonate systems. J Sed Res 77:572–586

Fredlund DG, Krahn J (1977) Comparison of slope stability methods of analysis. Can Geotech J 14:429–439

Fredlund DG, Krahn J, Pufahl DE (1981) The relationship between limit equilibrium slope stability methods. In: Proceedings, 10th international conference on soil mechanics and foundation engineering, Stockholm, Sweden, Balkema, Rotterdam, vol. 3, pp 409–416

Fryer GJ, Watts P, Pratson LF (2004) Source of the great tsunami of 1 April 1946: a landslide in the upper Aleutian forearc. Mar Geol 203:201–218

Gedik N, Irtem E, Kabdasli S (2005) Laboratory investigation on tsunami run-up. Ocean Eng 32:513–528

Geoscience Australia (2008) Offshore tsunami hazard for Australia. http://www.ga.gov.au/hazards/tsunami/offshore-tsunami-hazard-for-australia.html. Accessed 10 Jul 2012

Geoscience Australia (2012) Earthquake Database. http://www.ga.gov.au/earthquakes/searchQuake.do. Accessed 10 Jul 2012

Glenn K, Post A, Keene J, Boyd R, Fountain L, Potter A, Osuchowski M, Dando N, Shipboard Party (2008) NSW continental slope survey–post cruise report. Geoscience Australia, Record 2008/14, p 160

Grilli ST, Vogelmann S, Watts P (2002) Development of a 3D numerical wave tank for modeling tsunami generation by underwater landslides. Eng Anal Boundary Elem 264:301–313

Grilli ST, Watts P (2005) Tsunami generation by submarine mass failure. I: modelling, experimental validation, and sensitivity analyses. J Waterw Port Coast Ocean Eng 131:283–297
Haflidason H, Sejrup HP, Nygard A, Mienert J, Bryn P, Lien R, Forsberg CF, Berg K, Masson D (2004) The Storegga Slide: architecture, geometry and slide development. Mar Geol 213:201–234
Hampton MA, Lee HJ, Locat J (1996) Submarine landslides. Rev Geophys 34:33–59
Harbitz CB, Løvholt F, Pedersen G, Masson DG (2006) Mechanisms of tsunami generation by submarine landslides: a short review. Norw J Geol 86:255–264
Hsiao S-C, Hsu T-W, Lin T-C, Chang Y-H (2008) On the evolution and run-up of breaking solitary waves on a mild sloping beach. Coast Eng 55:975–988
Kawata Y, Benson BC, Borrero JC, Davies HL, De Lang WP, Imamura F, Letz H, Nott J, Synolakis CE (1999) Tsunami in Papua New Guinea was as intense as first thought. EOS Trans Am Geophys Union 80:101
Kayen RE, Lee HJ (1991) Pleistocene slope instability of gas hydrate-laden sediment on the Beaufort Sea margin. Mar Georesour Geotechnol 10:125–141
Koloski JW, Schwarz SD, Tubbs DW (1989) Geotechnical properties of geologic materials. In: Galster RW (ed) Engineering geology in Washington, vol 1. Wash Division Geol Earth Resour Bull 78
Leynaud D, Mienert J, Nadim F (2004) Slope stability assessment of the Helland Hansen area offshore the mid-Norwegian margin. Mar Geol 213:457–480
Li Y, Raichlen F (2003) Energy balance model for breaking solitary wave runup. J Waterw Port Coast Ocean Eng 129:47–59
McAdoo BG, Watts P (2004) Tsunami hazard from submarine landslides on the Oregon continental slope. Mar Geol 203:235–245
McPherson A, Allen T (2006) An improved understanding of earthquake groundshaking in Australia. In: Proceedings of the 2006 Australian Earthquake Engineering Society Conference, Canberra, Australia, pp 239–244
Middelmann MH (2007) Natural hazards in Australia. Identifying risk analysis requirements. Geoscience Australia, Canberra, p 173
Moore JG, Clague DA, Holcomb RT, Lipman PW, Normark WR, Torreesan ME (1989) Prodigious submarine landslides on the Hawaiian ridge. J Geophys Res 94:17465–17484
Nixon MF, Grozic JLH (2006) A simple model for submarine slope stability analyses with gas hydrates. Norw J Geol 89:309–316
Puga-Bernabéu Á, Webster JM, Beaman RJ, Guilbaud V (2011) Morphology and controls on the evolution of a mixed carbonate–siliciclastic submarine canyon system, Great Barrier Reef margin, north-eastern Australia. Mar Geol 289:100–116
Queensland Government, Environment and Resource Management (2007) Fact sheet Solomon Island tsunami, p 3 http://www.derm.qld.gov.au/register/p02118aa.pdf
Rabinovich AB, Thomson RE, Bornhold BD, Fine IV, Kulikov EA (2003) Numerical modelling of tsunamis generated by hypothetical landslides in the Strait of Georgia, British Columbia. Pure Appl Geophys 160:1273–1313
Ruff LJ (2003) Some aspects of energy balance and tsunami generation by earthquakes and landslides. Pure Appl Geophys 160:2155–2176
Rynn J, Davidson J (1999) Contemporary assessment of tsunami risk and implications for early warnings for Australia and its island territories. Sci Tsunami Hazards 17:107–125
Sexton J, Nielsen O, Burbidge D, Dhu T (2009) Scientific expertise and emergency management. Ausgeo News 93:1–3
Somerville P, Graves R, Collins N, Song S-G, Ni S, Cummins P (2009) Source and ground motion models for Australian earthquakes. In: Proceedings of the 2009 Australian Earthquake Engineering Society Conference, Newcastle, Australia
Sultan N, Cochonat P, Canals M, Cattaneo A, Dennielou B, Haflidason H, Laberg JS, Long D, Mienert J, Trincardi F, Urgeles R, Vorren TO, Wilson C (2004) Triggering mechanisms of slope instability processes and sediment failures on continental margins: a geotechnical approach. Mar Geol 213:291–321
Synolakis CE, Bardet J-P, Borrero JC, Davies HL, Okal EA, Silver EA, Sweet S, Tappin DR (2002) The slump origin of the 1998 Papua New Guinea Tsunami. Proc R Soc Lond 458:763–789
Tappin DR, Watts P, McMurtry GM, Lafoy Y, Matsumoto T (2001) The Sissano, Papua New Guinea tsunami of July 1998—offshore evidence on the source mechanism. Mar Geol 175:1–23
Terzaghi K (1950) Mechanisms of landslides. In: Paige S (ed) Application of geology to engineering practice. Geological Society of America, New York, pp 83–123
Tinti S, Zaniboni F, Armigliato A, Pagnon G, Gallazzi S, Manucci A, Brizuela B, Bressan L, Tonini R (2007) Tsunamigenic landslides in the western Corinth Gulf: numerical simulations. In: Lykousis V, Sakellariou D, Locat J (eds) Submarine mass movements and their consequences. Springer, Berlin, pp 405–414

Urgeles R, Locat J, Dugan B (2007) Recursive failure of the Gulf of Mexico continental slope: timing and causes. In: Lykousis V, Sakellariou D, Locat J (eds) Submarine Mass Movements and Their Consequences. Springer, Berlin, pp 209–219

Venkatesan S, Dhu T, Lam NTK, Wilson JL (2003) The effect of rock motion on soil amplification factors for Australian conditions. In: Proceedings of the Australian Earthquake Engineering Society, Ann Conference, Melbourne, paper 16, p 7

Ward SN (2011) Tsunami. In: Gupta H (ed) Encyclopedia of solid earth geophysics. Springer, Berlin, pp 1473–1492

Watts P, Grilli ST, Kirby JT, Fryer GJ, Tappin DR (2003) Landslide tsunami case studies using a Boussinesq model and fully nonlinear tsunami generation model. Nat Hazards Earth Syst Sci 3:391–402

Watts P, Grilli ST, Tappin DR, Fryer GJ (2005) Tsunami generation by submarine mass failure. II: predictive equations and case studies. J Waterw Port Coast Ocean Eng 131:298–310

Webster JM, Beaman RJ, Bridge TCL, Davies PJ, Byrne M, Williams S, Manning P, Pizarro O, Thornborough K, Woolsey E, Thomas AL, Tudhope A (2008a) From corals to canyons: the Great Barrier Reef Margin. EOS Trans Am Geophys Union 89:217–218

Webster JM, Davies PJ, Beaman RJ, William S, Byrne M (2008b) Evolution of drowned shelf edge reefs in the GBR; implications for understanding abrupt climate change, coral reef response and modern deep water benthic habitats. *RV Southern Survey—voyage summary*; Marine National Facility, p 18 http://www.marine.csiro.au/nationalfacility/voyagedocs/2007/summarySS07-2007.pdf

Webster JM, Yokoyama Y, Cotterill C, Expedition 325 Scientists (2011) Proceedings of the Integrated Ocean Drilling Program 325. doi:10.2204/iodp.proc.325.2011